Electronic supplemental information for:

Dissolution of Mn-bearing dolomite drives elevated Cr(VI) occurrence in a Permian redbed aquifer

Jeffrey P. Westrop, Zach Tomlinson, Brandon Maples, Kato T. Dee, Andrew L. Swindle, Megan E. Elwood Madden, Qinhong Hu, Andrew S. Elwood Madden

Table of Contents

Geologic map of the study area

Figure S1 (next page). The geologic map of a portion of the study area (adapted from [1]) to highlight the location of the Norman Arsenic Test Hole[2]. Aquifer rock samples used for chemical and mineralogical analysis were from the Norman Arsenic Test Hole Core.

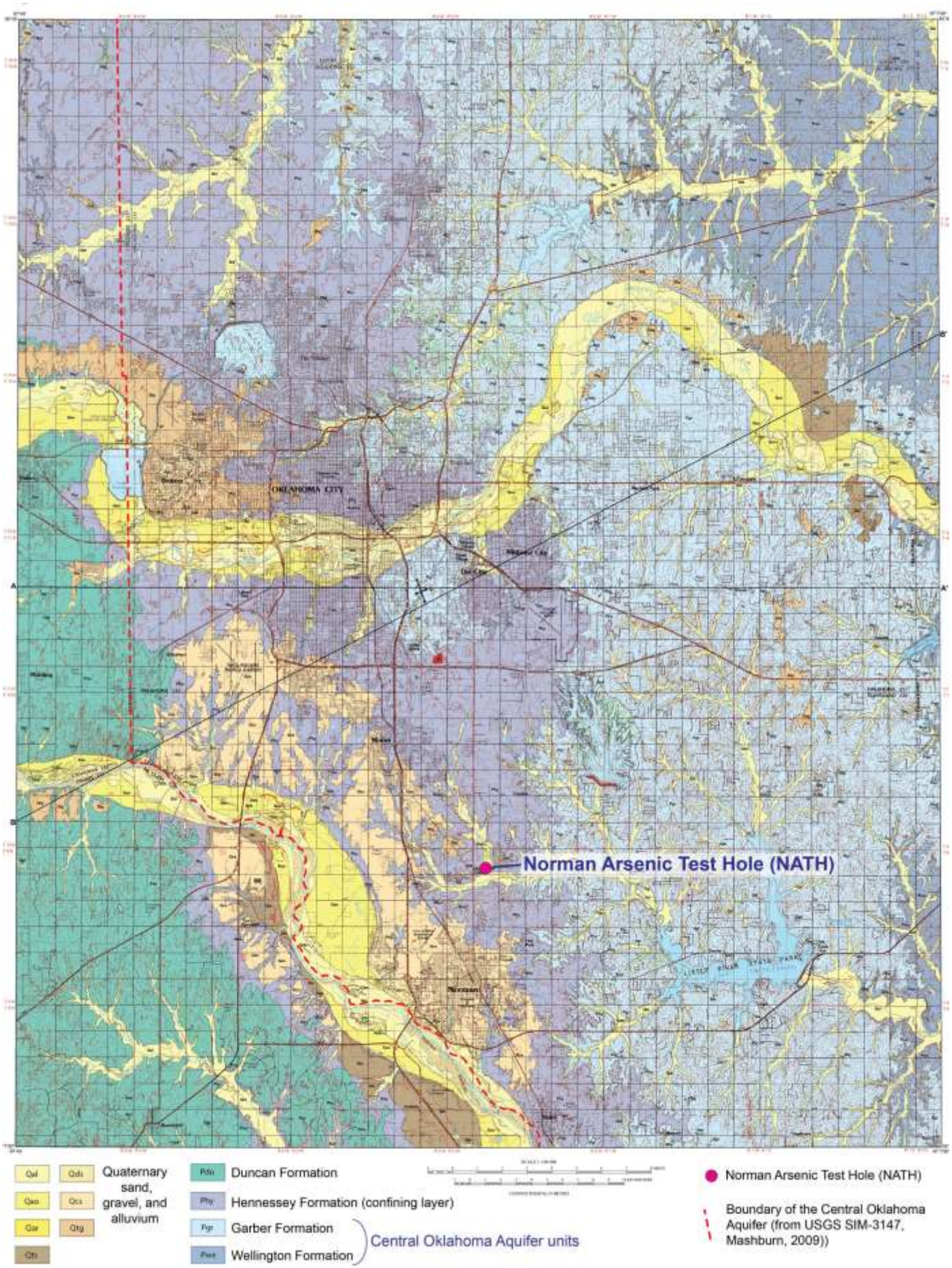
OKLAHOMA CITY
Norman Arsenic Test Hole (NATH)
Quaternary sand, gravel, and alluvium
Duncan Formation
Hennessey Formation (confining layer)
Garber Formation
Wellington Formation
Central Oklahoma Aquifer units
Norman Arsenic Test Hole (NATH)
Boundary of the Central Oklahoma Aquifer (from USGS SIM-3147, Mashburn, 2009))

Methods for statistical evaluation of groundwater data

Data as-received from the various databases was significantly reorganized to successfully perform analyses. Before doing any data processing, it is first necessary to determine the data types. Ellefsen, Smith, and Horton[3], Engle and Blondes[4], Fowler et al.[5], Garrett[6], Boogaart and Tolosana[7], etc. have all stated that geochemical data is compositional, which [requires special types of processing. Garrett[6] and van den Boogaart and Tolosana[7] define compositional data as a set of positive numbers (components) that sum up to a constant (the total). Our data (expressed in mmol/kg) may not seem to meet this requirement, but by multiplying by the molar weight of the solute it can easily be converted to ppm units, which must sum to 10^6. The mmol/kg unit simply does not appear to have a fixed sum because it is a ratio between the solute and water components, but that does not affect its compositional nature.

Once the nature of the data was addressed, we also had to determine what information to filter out for the actual clustering analysis. Since a main objective of the study required clustering by geochemistry, we only considered the pH (converted to H^+ concentration in mmol/L), Cr(VI) (converted to mmol/kg), CO_3^{2-} (mmol/L eq.), Ca^{2+}, Mg^{2+}, Cl^-, and SO_4^{2-} (all represented in mmol/kg). We removed the K^+ and SiO_2(aq) concentrations from consideration because 19.4% and 50.9% of the values were missing, respectively. Although multiple methods exist for filling in missing values, they could not be accurately applied to our data. One of the methods used by Cloutier et al.[8] was to average values from surrounding wells to fill missing entries. Most of the wells in our dataset with missing sample values had less than 3 nearby usable wells, as seen below. Less than 3 averaged values would make the means inaccurate. Additionally, the rapid lateral changes in lithology within the Garber-Wellington, documented in Ben Abbott's thesis work[9], would make averaging nearby well values potentially misleading (Figure S2).

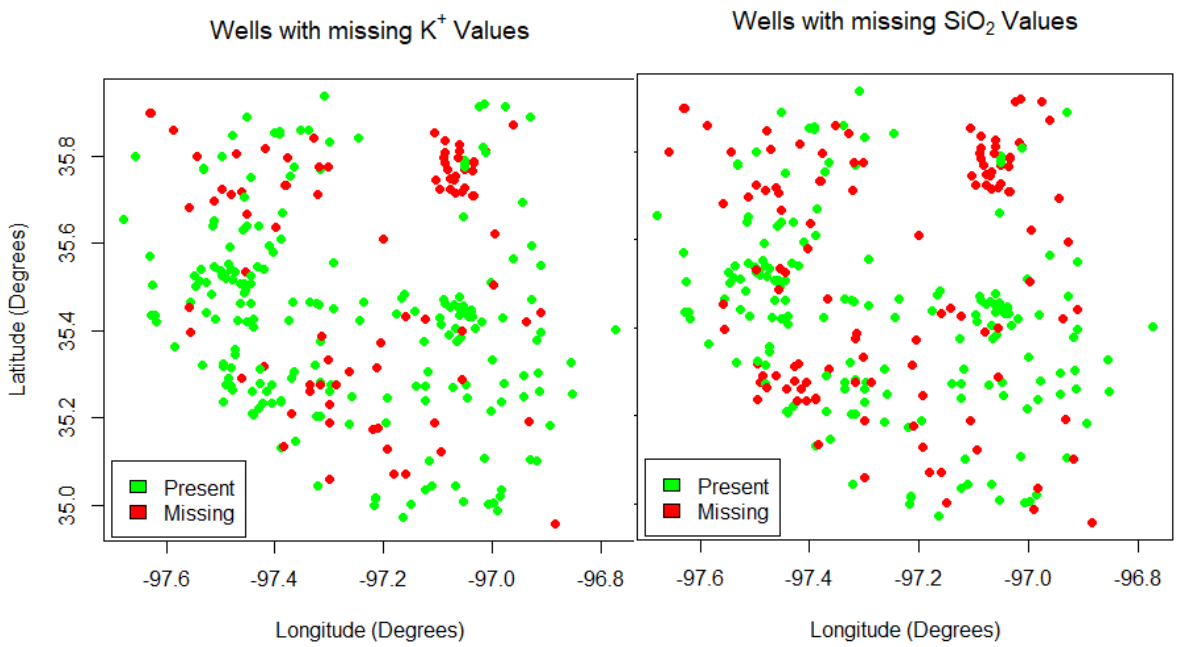

Figure S2. Spatial locations (map view) of data missing K^+ and SiO_2 (aq) values. We determined that nearby values were too sparse to consider adding predicted/estimated values; therefore these analytes were not included in the study.

Another common method fills missing at random (MAR) values based on the underlying distribution inferred from the available data, which can take many different forms[7]. With so much of the SiO_2 (aq) and K^+ data missing however, any natural partitions in the data could be easily obscured by whatever distribution model we used to calculate said values and limit the usefulness of the clustering.

A final method of filling in MAR values used by Cloutier et al.[8] was electro-neutrality; they calculated the missing value in the sample such that all the ions in the sample would be charge-balanced. We could not use electroneutrality because the dataset did not include all the ions present in the water samples. Out of 281 samples with both K^+ and SiO_2 (aq) concentrations, only 7 had an electro-neutrality within 10% of neutral, the cutoff point which Cloutier et al.[8] used to remove erroneous measurements. Because of the compositional nature of the data, however,

missing ions do not affect the analysis if the appropriate data processing methods are employed, which will be discussed below.

In addition to missing values, geochemical data often has concentrations which fall below the detection limits (dl's) of the methods used to measure them. Sophisticated methods for replacement usually require that the dataset be lognormally or normally distributed[10], but our data did not meet that requirement. Farnham et al.[10] simulated a data set and implemented variable dl's such that fixed percentages of the data would fall below the detection limits. They then used PCA to show that replacing the data which fell below the dl with half of the dl value produced results generally closer to the original matrix than replacing the data with 0 or the full dl value. Therefore, we replaced values which fell below detection limits with half of the dl value.

We then isometric log ratio (ilr) transformed the dataset. The ilr transformation is justified for geochemical data in many literature sources (e.g., [3, 4, 11]). The ilr is a transformation which provides the coordinates of a composition with respect to some orthonormal basis computed from the centered log ratio (clr) hyperplane[7]. This clr hyperplane (and, therefore, the ilr transformation) meets the required properties of compositional data; namely, scaling invariance and subcompositional coherence[7]. The property of scaling invariance states that the size of the sample is irrelevant, which is an obvious necessity for compositional data. Imagine getting two water samples: one 1 kg and one 500g. Let the 1 kg sample contain 0.2 mmol of Na^+. Let the 500 g sample contain 0.1 mmol of Na^+. Despite being outwardly different measurements, the two measurements clearly represent the same concentration. Subcompositional coherence essentially states that adding or subtracting components should not change the relationship between the data. Using a ternary diagram (or Piper plot) relies on subcompositional coherence because it

examines the relationships between only a few variables and requires that those results can be extrapolated to the full data set. In fact, the ilr transformation could be considered the x y coordinates of the points on a ternary diagram in a system that contains 3 components. Therefore, the ilr transformation occupies a D-1 dimensional space. Along the same analogy, the clr transformation takes the points from a ternary plot and projects them back into $\mathbb{R}^D$ but in an orthonormal basis which is also perpendicular to the v=<1, 1, . . . ,1> vector, the vector representing the center of any ternary plot[7]. Since both the clr and ilr transformation meet the requirements for compositional data, they are both readily used for data processing and have their own strengths and weaknesses.

The original data (from the NWIS dataset by USGS) had multiple measurements for some of the wells corresponding to different years and seasons. To avoid giving some of the wells large weights from being sampled more often, we averaged together all of the measurements that came from the same well at the same depth (in ilr space). There was no statistically significant difference in the spring vs. winter geochemistry at 95% confidence, which justifies averaging together the repeat measurements. We created a random sample of 30 wells that were sampled in both the late spring (May/June) and near winter (mostly November, January, and February). A hypothesis test on the null hypothesis that the mean spring geochemistry was equal to the mean summer geochemistry yielded a p-value of 0.9838, indicating that the null hypothesis could not be rejected at 95% confidence.

Once all of the repeat measurements were averaged together in ilr space, they were transformed back to real space and then to clr space for hierarchical cluster analysis. This processing method for cluster analysis is recommended by van den Boogaart and Tolosana[7], as clr transformation projects the compositional points into a coordinate system that can generate

effective euclidean distance matrices for the cluster analysis. Ward's method for linkage was used along with the euclidean distance calculations using the dist() and hclust() r functions. Five clusters were chosen because, based on the cluster dendrogram, 5 was the minimum number of clusters which kept within-cluster variation (measured as euclidean distance) relatively small. There is a large gap between the within-cluster variation for 5 or more clusters and less than 5 clusters. Despite the benefits of clr and ilr transformation in clustering, they destroy the original data structure and units; therefore, the original data was used to calculate descriptive statistics for the clusters.

Bulk chemistry of NATH core samples

Sample #	Depth (ft)	Cr (ppm)	U (ppm)	As (ppm)	Fe (%)	S (%)
1	303	30	0.9	11	1.1	0.01
2	322	110	2.6	7	2.7	0.01
3	331	90	2.0	12	2.5	0.01
4	334	50	1.2	0	0.9	<0.01
5	372	50	0.6	0	0.3	0.01
6	374	100	2.5	8	2.8	0.01
7	375	40	1.0	0	0.7	0.02
8	377	130	3.8	11	3.6	0.04
9	386	80	2.0	5	1.8	0.01
10	391	120	3.1	18	6.0	0.01
11	402	60	1.5	3	0.9	0.01
12	415	130	3.2	5	2.2	<0.01
13	420	20	0.4	0	0.3	<0.01
14	425	40	1.0	0	0.5	<0.01
15	429	80	1.9	0	0.4	<0.01
16	440	10	0.4	0	0.2	<0.01
17	443	60	1.6	7	1.4	<0.01
18	456	30	0.7	0	0.2	0.01
19	458	120	3.3	0	4.7	0.01
20	463	90	2.6	5	1.9	0.01
21	468	100	3.1	11	5.4	0.02
22	470	60	2.0	0	1.9	0.02
23	471	80	2.7	0	4.5	0.03
24	474	80	2.3	0	2.1	0.04
25	475	80	2.0	0	1.4	0.02
26	477	80	2.1	6	2.1	0.03
27	479	80	2.2	0	2.6	0.04
28	481	60	1.1	0	0.8	0.03
29	483	60	1.7	8	1.9	0.04
30	485	120	2.9	15	5.1	0.04
31	489	70	1.1	0	0.5	0.01
32	490	30	0.6	0	0.5	0.01
33	492	50	0.9	0	0.4	0.01
34	496	50	1.4	0	1.8	0.02
35	502	160	2.5	0	3.1	0.01
36	504	90	2.4	N/A	N/A	N/A
37	512	110	2.9	N/A	N/A	N/A
38	517	100	2.9	5	2.7	0.01
39	524	130	3.3	16	5.6	0.01
40	526	120	2.7	8	2.6	0.01
41	535	110	2.9	10	3.2	<0.01
42	571	40	0.8	0	0.3	<0.01
43	573	20	0.5	0	0.3	0.01
44	581	30	0.7	N/A	N/A	N/A
45	589	70	1.3	0	0.8	<0.01
46	595	60	1.7	N/A	N/A	N/A
47	642	20	0.5	0	0.3	<0.01
48	647	30	0.5	0	0.2	0.01
49	649	160	3.1	13	4.0	0.02
50	651	20	0.6	0	0.5	0.02

Table S1. Selected bulk chemical analyses of the core samples from the NATHC. Samples highlighted in grey are mudstones, while the samples in orange are sandstones, and samples in red are conglomerates. All tables displaying results from the NATHC follow this color scheme.

Mineralogy of NATH core samples by powder XRD

Sample #	Depth (ft)	% Qtz	% Clay	% Carb	% Plag	% K-spar	% Hem	% Anatase	Total
1	303	15.2	0.7	83.1	0.5	0.5	0	0	100
2	322	65.5	30	0	0	4	0.5	0	100
3	331	89.2	7.3	0	0	1.8	1.6	0	99.9
4	334	96.3	0.1	2.9	0	0	0.7	0	100
5	372	61.2	0	38.4	0	0.4	0	1	100
6	374	64.6	21.2	10.7	1.2	0.9	1.4	0	100
7	375	78.9	17	0	0.6	2.2	0.8	0.5	100
8	377	71.9	11	13.1	0	2.7	1.1	0	99.8
9	386	72.6	26.2	0	0	0.8	0.4	0	100
10	391	41.8	51.6	0	0.3	1.2	2.5	2.5	99.9
11	402	82.6	14.3	0	1.2	1.4	0.5	0	100
12	415	81.2	16.9	0	1.1	0.5	0.3	0	100
13	420	75.1	23.8	0.3	0.4	0.3	0.1	0	100
14	425	88.5	9.9	0	0.7	0.3	0.7	0	100.1
15	429	97.7	0.3	0	0.8	1	0.2	0	100
16	440	97.5	0.6	0.6	0.8	0.7	0	0	100.2
17	443	82.6	15.1	0.2	1	0.6	0.5	0	100
18	456	81.9	3.8	12.7	0.8	0.5	0.1	0	99.8
19	458	39.6	48.7	0	8.4	2.3	0.9	0	99.9
20	463	80.6	15.3	0	1.5	2.1	0.4	0	99.9
21	468	52.5	34.7	0.5	0	4.4	7.9	0	100
22	470	72.2	21.7	0	0.6	5.2	0.3	0	100
23	471	66.9	25	3.4	1.8	1.3	1.5	0	99.9
24	474	24	11.3	62.2	1.1	0.7	0.4	0	99.7
25	475	77.5	15.3	0	2.3	5	0	0	100.1
26	477	73.4	24.4	1	0	1.2	0	0	100
27	479	62.9	30.8	0.1	3.1	1.9	0.1	1	99.9
28	481	84.6	7.7	0	4.9	2.2	0.4	0.1	99.9
29	483	68	26.9	0	3.4	1	0.7	0	100
30	485	67	26.7	0	4.7	1.2	0.6	0	100.2
31	489	94.4	2.1	1.4	1.4	0.5	0.2	0	100
32	490	93.4	0.7	4.8	0.9	0	0.3	0	100.1
33	492	97.1	1	1.2	0.7	0.1	0	0	100.1
34	496	91.7	7.1	0.2	0.4	0	0.6	0	100
35	502	67.5	29.3	0	0.2	1.3	1.1	0.5	99.9
36	504	70.8	26.1	0	1.6	0.5	0.9	0	99.9
37	512	55.9	38	0	4.3	1.3	0.6	0	100.1
38	517	57.1	40.4	0.3	1.3	0.5	0.5	0	100.1
39	524	40.8	47.7	0	6.3	0.4	3.3	1.5	100
40	526	64.2	28.8	0	3.3	1	1.9	0.9	100.1
41	535	75.2	21.4	0	1.3	1.3	0.5	0.4	100.1
42	571	95.4	3.2	0	1	0.3	0.2	0	100.1
43	573	74.2	1.2	24.3	0	0.2	0.1	0	100
44	581	95.9	1.9	1.5	0.3	0.3	0	0	99.9
45	589	90.9	5.3	2.2	0.7	0.7	0.3	0	100.1
46	595	72.9	9.2	15.9	0.4	1	0.7	0	100.1
47	642	99	0.5	0	0.3	0.1	0.1	0	100
48	647	97.6	1.9	0	0.4	0	0.1	0	100
49	649	61	32.8	0	0.2	1.4	4.7	0	100.1
50	651	72.3	1.6	25.7	0	0.3	0.2	0	100.1

Table S2. Bulk XRD results for the core samples.

Sample #	Depth (ft)	% Clay	% Kaol	% Mica/ illite	% Chl	% Carb	% Dol	% Ank	% Cal
1	303	0.7	0.7	0	0	83.1	83.1	0	0
2	322	30	18	12	0	0	0	0	0
3	331	7.3	1.9	5.4	0	0	0	0	0
4	334	0.1	0.1	0	0	2.9	0	2.9	0
5	372	0	0	0	0	38.4	1.3	0	37.1
6	374	21.2	12.8	8.4	0	10.7	10.7	0	0
7	375	17	8.1	8.9	0	0	0	0	0
8	377	11	9	2	0	13.1	10.6	0	2.5
9	386	26.2	10	13.7	2.5	0	0	0	0
10	391	51.6	39.3	12.3	0	0	0	0	0
11	402	14.3	5.6	7.9	0.8	0	0	0	0
12	415	16.9	15.1	1.8	0	0	0	0	0
13	420	23.8	1.3	22.5	0	0.3	0.3	0	0
14	425	9.9	5.1	4.8	0	0	0	0	0
15	429	0.3	0.1	0.2	0	0	0	0	0
16	440	0.6	0.4	0.2	0	0.6	0.6	0	0
17	443	15.1	11.3	3.8	0	0.2	0.2	0	0
18	456	3.8	3.8	0	0	12.7	12.4	0	0.3
19	458	48.7	29.9	15	3.8	0	0	0	0
20	463	15.3	13.2	1.3	0.8	0	0	0	0
21	468	34.7	9.3	22.3	3.1	0.5	0.5	0	0
22	470	21.7	10.3	5.2	6.2	0	0	0	0
23	471	25	9	15.6	0.4	3.4	3.4	0	0
24	474	11.3	4.4	6.8	0.1	62.2	45.9	16.3	0
25	475	15.3	13.5	0.7	1.1	0	0	0	0
26	477	24.4	9	15.4	0	1	1	0	0
27	479	30.8	6	24.8	0	0.1	0.1	0	0
28	481	7.7	2.6	3.4	1.7	0	0	0	0
29	483	26.9	15.2	7	4.7	0	0	0	0
30	485	26.7	8.6	11.6	6.5	0	0	0	0
31	489	2.1	1	1.1	0	1.4	0.9	0	0.5
32	490	0.7	0.7	0	0	4.8	2	0	2.8
33	492	1	0.4	0.6	0	1.2	1.2	0	0
34	496	7.1	5.5	1.6	0	0.2	0.1	0	0.1
35	502	29.3	17.7	8.8	2.8	0	0	0	0
36	504	26.1	10.4	13.2	2.5	0	0	0	0
37	512	38	13.9	20.5	3.6	0	0	0	0
38	517	40.4	5	14.6	20.8	0.3	0.3	0	0
39	524	47.7	28.1	19.6	0	0	0	0	0
40	526	28.8	11.4	17.4	0	0	0	0	0
41	535	21.4	8	13.4	0	0	0	0	0
42	571	3.2	2.1	1.1	0	0	0	0	0
43	573	1.2	0.6	0.6	0	24.3	0	0	24.3
44	581	1.9	1.2	0.7	0	1.5	1.5	0	0
45	589	5.3	3.1	2.2	0	2.2	2.2	0	0
46	595	9.2	6	3.2	0	15.9	15.9	0	0
47	642	0.5	0.5	0	0	0	0	0	0
48	647	1.9	1.9	0	0	0	0	0	0
49	649	32.8	18.8	14	0	0	0	0	0
50	651	1.6	1.1	0.5	0	25.7	25.7	0	0

Table S3. Detailed Clay and Carbonate bulk XRD results

Separates % clay into % kaolinite, % illite, and % chlorite, and % carbonate into % dolomite, % calcite, and % ankerite.

Detailed results from NATH core chemical extractions

Sample	Depth	Net Cr ox (ppb)	UPW Cr AA (ppb)	PO4 Cr AA (ppb)	HHCl Cr AA (ppb)	6N HCl AA (ppb)	Mn Oxides (ppm)
1	322	35	BDL	47	BDL	758	93
2	373	8	BDL	45	6	139	3520
3	376	20	3	52	BDL	687	365
4	402	111	2	45	1	377	55
5	420	252	BDL	31	10	22	292
6	429	114	BDL	38	BDL	116	74
7	473	140	1	46	3	438	4635
8	479	69	BDL	22	BDL	954	29
9	485	51	6	53	BDL	1058	175
10	502	13	BDL	53	4	2031	25
11	535	25	2	55	14	890	382
12	584	204	BDL	44	7	269	291
13	595	59	3	59	BDL	717	156
14	642	228	5	42	BDL	827	113

Table S4. Results from chemical extractions. "Mn-oxides" corresponds to the Mn value of the supernatant of the selective Mn-HHCl extraction. The table is color-coded based on lithology. BDL="below detection limit".

EPMA and SEM-EDXA data

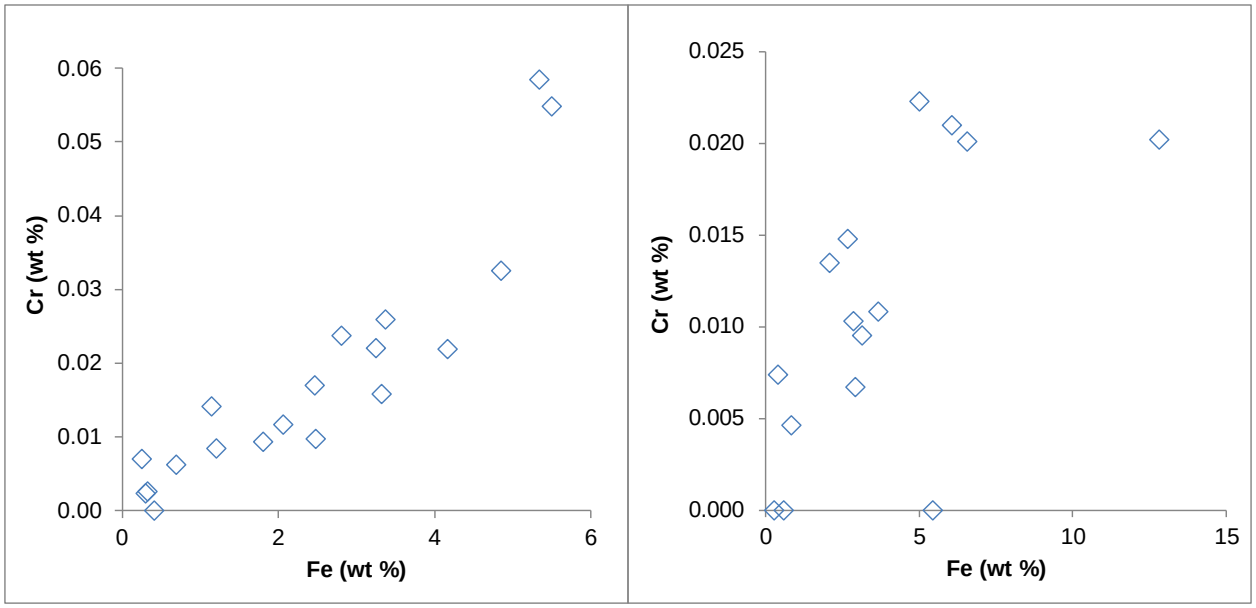

Fig. S3. Calculated wt.% values calculated from Wavelength-Dispersive X-ray Spectroscopy (WDS) for individual points determined via EPMA on Norman Arsenic Test Hole (NATH) core samples from 323 ft deep (left) and 502 ft deep (right).

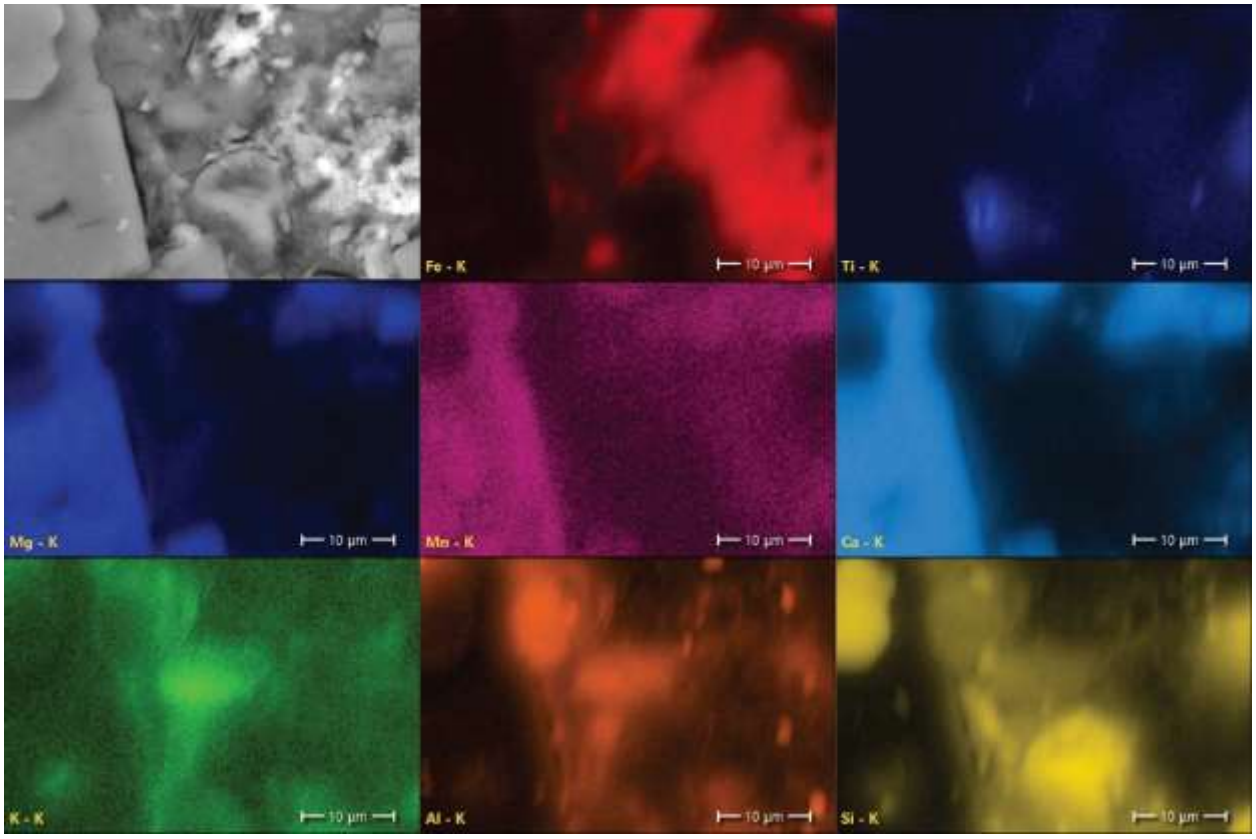

Figure S4. Backscattered electron image (upper left) and energy-dispersive X-ray analysis elemental maps (other panels, labelled with element of interest) collected on a thin section sample from the Norman Arsenic Test Hole core at 591 ft. depth. detailing a of a region showing a pore next to dolomite in Mn is enriched both in the relatively coarse-grained Mg-Ca rich dolomite area to the left in addition to the fine-grained Fe-enriched pore filling material that includes Fe, Mn oxides and clays.

References cited

1. T. M. Stanley and G. R. Standridge, Geologic map compilation of the Oklahoma City Metro Area, Central Oklahoma.*Journal*, 2008, OGQ-74.
2. J. Smith, S. Paxton, S. Christenson, R. Puls and J. Greer, Flow Contribution and Water Quality with Depth in a Test Hole and Public-supply Wells: Implications for Arsenic Remediation Through Well Modification, Norman, Oklahoma, 2003-2006, *U.S. Environmental Protection Agency, Office of Research and Development, National Risk Management Laboratory*, 2009.
3. K. J. Ellefsen, D. B. Smith and J. D. Horton, A modified procedure for mixture-model clustering of regional geochemical data, *Applied Geochemistry*, 2014, **51**, 315-326.
4. M. A. Engle and M. S. Blondes, Linking compositional data analysis with thermodynamic geochemical modeling: Oilfield brines from the Permian Basin, USA, *Journal of Geochemical Exploration*, 2014, **141**, 61-70.
5. A. Fowler, N. Spycher, R. A. Zierenberg and C. A. Cantwell, Identification of blind geothermal resources in Surprise Valley, CA, using publicly available groundwater well water quality data, *Applied Geochemistry*, 2017, **80**, 24-48.
6. R. G. Garrett, The 'rgr' package for the R Open Source statistical computing and graphics environment - a tool to support geochemical data interpretation, *Geochemistry: Exploration, Environment, Analysis*, 2013, **13**, 355-378.
7. K. G. v. d. Boogaart and R. Tolosana-Delgado, Analyzing Compositional Data with R, 2013, DOI: 10.1007/978-3-642-36809-7.
8. V. Cloutier, R. Lefebvre, R. Therrien and M. M. Savard, Multivariate statistical analysis of geochemical data as indicative of the hydrogeochemical evolution of groundwater in a sedimentary rock aquifer system, *J Hydrol*, 2008, **353**, 294-313.
9. B. N. Abbott, M.S. thesis, Oklahoma State University, 2005.
10. I. M. Farnham, A. K. Singh, K. J. Stetzenbach and K. H. Johannesson, Treatment of nondetects in multivariate analysis of groundwater geochemistry data, *Chemometrics and Intelligent Laboratory Systems*, 2002, **60**, 265-281.
11. H. Iwamori, K. Yoshida, H. Nakamura, T. Kuwatani, M. Hamada, S. Haraguchi and K. Ueki, Classification of geochemical data based on multivariate statistical analyses: Complementary roles of cluster, principal component, and independent component analyses, *Geochemistry, Geophysics, Geosystems*, 2017, **18**, 994-1012.